European Commission

Horizon 2020
European Union funding
for Research & Innovation

REDUCTION OF RADIOLOGICAL ACCIDENT CONSEQUENCES

Action	Research and Innovation Action NFRP-2018-1
Grant Agreement #	847656
Project name	**R**eduction of **R**adiological **C**onsequences of design basis and design extension **A**ccidents
Project Acronym	R2CA
Project start date	01.09.2019
Deliverable #	D5.2.
Title	Report on innovative diagnosis tools and devices
Author(s)	Karine Chevalier-Jabet, François Kremer (IRSN)
Version	01
Related WP	WP5 INNOV
Related Task	T5.2. Innovative diagnosis tools and devices (IRSN)
Lead organization	IRSN
Submission date	04.12.2023
Dissemination level	PU

This project has received funding from the Euratom research and training programme 2014-2018 under the grant agreement n° 847656

History

Date	Submitted by	Reviewed by	Version (Notes)
04.12.2023	K. Chevalier-Jabet, F. Kremer (IRSN)	N. Girault (IRSN)	01

Abbreviations

ANN	Artificial Neural Network
GTRF	Grid-To-Rod-Fretting
FP	Fission Product
PCC	Pearson Correlation Coefficient
PWR	Pressurized Water Reactor
SA	Sensitivity Analysis
SCC	Stress Corrosion Cracking
UQ	Uncertainty Quantification
VIF	Variance Inflation Factor

Contents

1. Introduction

During normal reactor operations, the fuel cladding acts as a barrier to prevent the fission products (FP) generated within the nuclear fuel to be released to the reactor primary circuit. Some part of fission gases and volatile FP may be released from the fuel matrix (~5-10% at rod average burnups of 50 GWd/tU (Manzel & Walker, 2002)), but they are retained within the fuel-cladding gap as long as the cladding layer is intact. The fuel cladding may, however, be damaged during reactor operations due to the influence of various phenomena, such as stress corrosion cracking (SCC), grid-to-rod fretting (GTRF), debris induced failure, among others (Kim & Kim, 2012). Over the years, with improved knowledge and best practices for fuel fabrication and design, the probability of fuel failure has however been reduced to low levels. For the Pressurized Water Reactors (PWR), the worldwide fuel rod defect rate between 2006 and 2015 was typically around 0.004% (IAEA, 2019). Even with such low defect rates, it remains of significant importance to understand and study the radioactive FP release from defected fuels as it can cause an increase of the primary circuit contamination and radiation exposure risks.

If a water-cooled nuclear reactor (like PWR) is operated under the defective conditions, the high-pressure coolant water can enter the fuel-to-clad gap through the defect site causing the FP retained within the gap to escape into the primary coolant (Awan et al., 2011; Lewis, 1988). Furthermore, the water steam in the defective fuel elements can cause the oxidation of the fuel, which may further enhance FP release (Higgs et al., 2007; Lewis, 1990). Moreover, some of the released radionuclides can also interact with the coolant and may cause serious corrosion problems to the fuel cladding or other reactor structures. Finally, further deterioration of the defective fuel elements can also occur with continued operation due to internal secondary hydriding of the Zircaloy cladding (Lewis et al., 1993). Such deterioration is massive can lead to blister formation throughout the clad leading to a once-through clad defect and potential clad rupture. The subsequent increased activity release may affect the power plant economically, caused by the lost burnup due to an early discharge of the fuel at power.

The increase of activity in the reactor coolant is an indicator of the onset of defect and is used to estimate the number and failure type of defective fuel rods. This increase can be attributed to the radioactive FP release and transport from the defective fuel to the reactor coolant. The FP release is usually considered in two stages: the release of radioactive FP from the fuel to the gap, and the release of such FP from the gap into the coolant through the defects in the cladding (Chun et al., 1998). FP release models developed to understand and analyse the FP transport from the fuel to the primary circuit adopt either the diffusion modelling approach or the first-order kinetic modelling approach, or both. These models generally employ a 'Booth-diffusion' type model (Booth, 1957) for release from the fuel matrix into the fuel-to-sheath gap (Lewis et al., 2007) and a first-order kinetic model to account for the transport and release of FP from the gap into the primary coolant (Iqbal et al., 2008; Kim & Kim, 2012). Several models have been developed for FP transport and fuel-failure evaluation. A few among them for the light water reactors include: (i) MERLIN, used by Electricité de France (EDF) (Tigeras Menéndez et al., 2009)), (ii) CADE, used by Westinghouse for PWRs (Burman et al., 1991). A comprehensive review of other models can be found in (Lewis et al., 2017) and (Dong et al., 2019).

The different approaches that have been adopted for fuel failure detection include: (i) using the operating limit of the specific activity in the coolant (Lusanova et al., 2001); (ii) using the release to birth ratio (R/B) slope versus decay constant in a log-log figure (Zanker, 1989); (iii) using the fitted escape rate coefficient, which directly represents the degree of fuel failure (Lewis et al., 2017). Some of the drawbacks associated with these methods were pointed out by (Dong et al., 2020). Using the operating limit of the specific activity in the coolant leads to delay from the time of fuel failure to the time the operating limit is reached, while the disadvantage of R/B slope method is that the slope is sensitive to fuel rod power and therefore this method lacks generality (Tigeras Menéndez, 2009). The fitted escape rate coefficient method, on the other hand, requires the operation history of the reactor and is vulnerable to the tramp uranium. The radioactivity ratio of two FP with different half-lives (Li et al., 2017; Tigeras Menéndez, 2009) is the most commonly used method for fuel failure detection.

Some data-driven methods, especially machine learning and deep learning approaches for fuel defect detection have gained momentum in the recent years. Artificial neural network (ANN) is one such machine learning approach that enables to establish a connection between the input parameters and the targets and can be a very efficient tool to make predictions about defected fuels. A general review of the state-of-the-art in ANN applications can be found in (Abiodun et al., 2018). The advantages of using the ANN method over the radioactivity (isotopic) ratios method are that it is more resistant to errors contributed by the tramp uranium and is more responsive when the fuel cladding is ruptured (Dong et al., 2020). ANN have been used quite extensively for several nuclear engineering applications. (Andrews et al., 1999) used ANN models to predict the release of volatile fission products from both CANDU and LWR fuel under severe accident conditions. The prediction of fuel rod failure by Pellet-Clad Interaction (PCI) was studied using the method of radial basis function neural network by (Wei et al., 2016). (Tayefi & Pazirandeh, 2014) used a Hopfield neural network to optimize fuel rod loading patterns in VVER/1000 reactors.

ANN models have also been used specifically for fuel failure detection during nuclear reactor operation. (Likhanskii et al., 2006) used ANN for fuel failure detection in the VVER reactor. (Wallace et al., 2020) recently demonstrated the application of neural network models for defect detection in the CANDU fuels. The approach was found to be relatively faster than the existing processes. It used an ANN method for fuel failure detection with the input of the ANN being the specific activities of FP in the primary coolant and the output being the degree of failure of the fuel cladding.

In this paper, a new fission product release and coolant activity calculation model is presented. The main objective of this physical model is to be used in conjunction with an artificial neural network for the diagnosis and characterization of defected fuel rods. This preliminary physical model, in its current state, may ignore some of the physical phenomena which occur in the different regions, such as the pellet, fuel-to-clad gap and the coolant. It was mainly developed to build the prototype of the expert system based on a neural network and to verify its applicability and efficiency for the prediction of defective fuel rods. It would be updated to account for such phenomena in the future.

The physical model was used to generate the computational database for the ANN to train on. In the process, the sensitivity analysis of the model parameters was also carried out to identify the ones which influence the output the most. The ANN was trained on the database and then tested on a separate never-seen-before data to make predictions of coolant activity and further determine the defect status (i.e., the presence of a defect or not). The preliminary results of predictions made with the ANN are presented in this report. A more detailed analysis using neural networks and updated physical model is foreseen for the future.

2. Physical Model for FP release

The physical processes of FP release from a defected fuel rod can be understood as a three-step process: (1) generation and transport of FP in the fuel pellet, (2) transport in the fuel-cladding gap, (3) transport in the coolant. Diffusion is considered as the main mechanism for the transport of FP in the fuel matrix and, thus, a diffusion model approach is adopted for the transport in the pellet region. The transport of FP in the fuel-to-clad gap can be quite complex, due to the chemistry of the isotopes as well as their interaction with the cladding. A generalized diffusion and first-order kinetic model were used in the gap region. The transport of FP in the primary coolant is modelled using the first-order kinetic model approach. The transport mechanisms in the three regions and the corresponding mass balance equations are presented in detail in the following sessions.

2.1. Fission Product transport in the Pellet

The FP transport process in the fuel pellet is dominated by mechanisms such as recoil, knockout and diffusion. Recoil release is a phenomenon in which a high energy fission fragment generated within a layer equal to the range of the fission fragments in fuel (~10 μm) can be released directly from the pellet surface before its kinetic energy is depleted (Olander, 1976). Knockout release, on the other hand, occurs when fission fragments collide with the crystal lattice atoms, transferring their energy to the atoms. These knock-ons can occasionally be fission

product atoms which would be released from the fuel matrix (Lewis, 1987; Olander, 1976). Both recoil and knockout release are athermal processes (dominant below about 1000°C). The other release mechanism is diffusion, by which fission fragments migrate to the grain boundary driven by a concentration gradient. Such migration of fission gases in the grain to the grain boundary via bubbles was modelled recently in (Verma et al., 2020). Once the bubbles reach the grain boundary and are interlinked, they provide a pathway for the FP to be released to the open porosities. This delaying phenomenon is, however, not considered in the present model.

Analytical expressions for the recoil and knockout processes are presented in (Lewis, 1987) who concluded that the release of the short-lived isotopes by knockout is of little importance compared to that of recoil. For this reason, knockout release has been neglected and the release by recoil and diffusion have been considered as the main release mechanisms in the present model.

The mass balance equation for the fission product transport in the pellet region can be thus expressed as:

$$\frac{dN_{f,i}}{dt} = FY_iP_{lin}l - \lambda_i N_{f,i} - R_{rec} - R_{diff}$$

Equation 1

where,
$N_{f,i}$ is the number of atoms of radionuclide 'i' in the fuel pellet region,
F is the fission rate in $fissionW^{-1}s^{-1}$,
Y_i is the independent fission yield of radioisotope i in $fission^{-1}$,
P_{lin} is the average linear power in Wm^{-1},
l is the effective fuel length in m,
λ_i is the decay constant of radioisotope i in s^{-1},
R_{rec} is the recoil release rate in s^{-1},
R_{diff} is the diffusion release rate in s^{-1}.
The first term on the right hand side of Equation 1 is the birth rate (s^{-1}) of FP in the fuel pellet, which will be denoted by 'B' in the following discussions:

$$B = FY_iP_{lin}l$$

The expression for the release to birth ratio (R/B) for the recoil release is adopted from (Lewis, 1987) as:

$$\left(\frac{R}{B}\right)^{rec} = \epsilon_{rec}\left(\frac{S_g}{V}\right)\mu_f$$

where,
ϵ_{rec} is the release efficiency, which is the probability for a fission fragment to stop in the gas-filled gap,
S_g is the geometrical surface area of the solid of volume V,
μ_f is the range of fission fragments in the fuel.
The constant ϵ_{rec} can be estimated as:

$$\epsilon_{rec} = \frac{V_c}{S_c\mu_g} = \frac{d_{gap}}{2\mu_g},$$

where,
(V_c/S_c), is the volume to surface ratio of the gas-filled gap,
μ_g is the range of fission fragments in the gap,
d_{gap} is the thickness of the radial gap.
So the recoil release can be evaluated as:

$$R_{rec} = \frac{d_{gap}}{R_{pel}} \frac{\mu_f}{\mu_g} * B$$

Equation 2

For the diffusion release within the fuel pellet, we use the well-known expression (Beck, 1960; Lewis & Husain, 2003) for the release to birth ratio as:

$$\left(\frac{R}{B}\right)^{diff} = \frac{3}{R_{gr}} \sqrt{\frac{D_i}{\lambda_i}} \left(coth \sqrt{\frac{\lambda_i R_{gr}^2}{D_i}} - \sqrt{\frac{D_i}{\lambda_i R_{gr}^2}} \right)$$

where,
R_{gr} is the radius of the grain ($\approx 5\mu$m),
D_i is the diffusion coefficient of the FP in the fuel matrix in $m^2 s^{-1}$,
λ_i is the decay constant of radioisotope i in s^{-1}
So the diffusion release can be evaluated as:

$$R_{diff} = B * \left(\frac{R}{B}\right)^{diff}$$

Equation 3

Here, the birth rate, B, also consists of the contribution of the transmutation of fission products. The most common used diffusion coefficient formula which involves the high, intermediate and low-temperature effects was proposed by (Turnbull et al., 1982) as:

$$D = 7.6 * 10^{-11} \exp\left(\frac{-35000}{T}\right) + 1.41 * 10^{-25} \sqrt{\dot{F}} \exp\left(\frac{-13800}{T}\right) + 2 * 10^{-40} * \dot{F}$$

where, T is the pellet centerline temperature in K, and $\dot{F}$ is the reaction rate in $m^{-3} s^{-1}$.
The total release rate from the pellet to the gap is then the sum of the recoil (Equation 2) and diffusion (Equation 3) release rates.

$$R_{f,i} = R_{rec} + R_{diff}$$

Equation 4

2.2. Fission Product transport in the fuel-to-clad gap

As mentioned before, when the fuel cladding is defective, the coolant can enter the gap and flash into water steam. Due to the pressure pulsation caused by the flashing and occurrence of steam-oxidation of the UO_2 fuel, the release of the FP can be enhanced (Lewis & Bonin, 1995). However, this transient release, which occurs instantaneously after defect onset, is not considered in the present study and only the long-term steady state release is analysed. Once the pressure in the gap is stable, FP release reaches this steady state. The FP released from the pellet are transported axially by diffusion through the free volumes of the rod and eventually reach the defect location where they can be released to the coolant.

Although the kinetic model, which assumes that FP release is a first-order kinetic process, similar to the decay process, has been used traditionally for the FP migration in the gap (Koo et al., 1994; Lewis et al., 1986), it cannot be adequately applied to all isotopes (Veshchunov, 2019). The two limiting cases of long-lived and short-lived isotopes can be reasonably described by the first-order kinetic model approach; however, an intermediate range of isotopes is controlled by the diffusion mass transfer in the gap. In that case the rate-determining process of transport in the gap was suggested to be the atomic diffusion of fission gases in a bulk steam environment (Lewis & Bonin, 1995), (Lewis et al., 1986). However, as the diffusion model did not allow an adequate description of the experimental observations, (Lewis et al., 1990) developed a generalized model which provided a unification of the previous diffusive and first-order kinetic approaches by considering axial diffusion along the gap in which release into the coolant was modelled as a surface-exchange process.
For a defect located at the middle of the length of cladding, the release rate from the gap into the coolant can be calculated as (Lewis et al., 1990):

$$R_{g,i} = \frac{2L_i}{l}\alpha\left[\frac{tanh\left(\frac{l}{2L_i}\right)}{\left(\frac{D_i}{L_i}\right)tanh\left(\frac{l}{2L_i}\right)+\alpha}\right]R_{f,i}$$

where,
$R_{g,i}$ is the rate of release of radionuclide i from the gap to the coolant in s^{-1},
L_i is the diffusion length of isotope i in m, with $L_i = \sqrt{D_i/\lambda_i}$,
α is the surface exchange coefficient,
l is the effective fuel length in m,
D_i is the diffusion coefficient of isotope i in high-pressure steam medium in $m^2 s^{-1}$,
$R_{f,i}$ is the release rate of radionuclide i from the fuel pellet to the gap in s^{-1}
Similarly, for a defect located at one end of the cladding, we get the expression:

$$R_{g,i} = \frac{L_i}{l}\alpha\left[\frac{tanh\left(\frac{l}{L_i}\right)}{\left(\frac{D_i}{L_i}\right)tanh\left(\frac{l}{L_i}\right)+\alpha}\right]R_{f,i}$$

(Veshchunov, 2019) improved the generalized model of Lewis and concluded that the explicit calculation of the escape rate coefficient becomes the key issue for further development and application of the generalized model or even the simplified first-order kinetic model, wherein it was being determined semi-empirically. From Veshchunov's consideration, the escape rate constant can be evaluated as:

$$\tilde{\varepsilon} = \tilde{\beta} = \frac{\beta}{l}$$

where, β is a surface exchange kinetic constant parameter (similar to α in Lewis' model) and is evaluated using the expression:

$$\beta = \frac{q_g l k T_{cl}^{(ext)}}{P_g^*}$$

Equation 5

where,
q_g is the release rate of stable non-condensable gases from the fuel to the gap in $m^{-3}s^{-1}$,
l is the effective fuel length in m,
k is the Boltzmann constant ($1.38 * 10^{23} JK^{-1}$),
$T_{cl}^{(ext)}$ is the cladding external temperature in K,
P_g^* is the critical value of the non-condensable gas partial pressure, at which release of gas into the coolant starts.

This critical value of partial pressure, P_g^*, is attained as a result of the gas-liquid film interface relocating towards the cladding surface where the steam partial pressure reaches the value $P_{H_2O}^{(eq)}\left(T_{cl}^{(ext)}\right)$. P_g^* is then obtained as:

$$P_g^* = P_{int} - P_{H_2O}^{(eq)}\left(T_{cl}^{(ext)}\right)$$

where, P_{int} is the internal pressure of the gap in Pa.
For the evaluation of β, apart from P_g^*, it is necessary also to estimate q_g. Now, q_g is calculated by the release rate of the stable fission gases from the fuel to the gap. However, it was noted by (Veshchunov, 2019), that the generation rate of non-condensable gases could be underestimated by not taking into account other sources of non-condensable gases such as hydrogen. Indeed, hydrogen can be generated in a defected fuel rod by mechanisms such as fuel oxidation by steam and hydrogen peroxide, radiolysis of water, and Zr alloy corrosion (Lewis et al., 1993, 2002). Their estimations lead to $q_{H2} \approx 10^{21} - 10^{23} m^{-3} s^{-1}$ which is quite higher than the estimates of q_g in (Veshchunov, 2019). So, hydrogen generation turns out to be the dominant mechanism for accumulation of stable non-condensable gas in the gap and we can replace q_g with q_{H2} in (Equation 5) for estimating β.

Therefore, using (Veshchunov, 2019) methodology to explicitly obtain the escape rate coefficient (by evaluating β), we can get the expression for the release rate of a radioisotope i from the gap to the coolant, by replacing α in expression by β as:

$$R_{g,i} = \frac{L_i}{l}\beta\left[\frac{tanh\left(\frac{l}{L_i}\right)}{\left(\frac{D_i}{L_i}\right)tanh\left(\frac{l}{L_i}\right)+\beta}\right]R_{f,i}$$

In order to take into account the different locations of the defect along the cladding length, we consider the fuel length to be divided into two sections such that the first section is from one end to the defect location and the other from the defect location to the other end (See Figure 1). Then the expression for the defect at one end location can be superimposed with the expression for the defect at the other end. If l is the total effective length and the defect is located at l_d from one end, then the release rate becomes:

$$R_{g,i} = \frac{L_i}{l}\beta\left[\left(\frac{tanh\left(\frac{l_d}{L_i}\right)}{\left(\frac{D_i}{L_i}\right)tanh\left(\frac{l_d}{L_i}\right)+\beta}\right)+\left(\frac{tanh\left(\frac{l-l_d}{L_i}\right)}{\left(\frac{D_i}{L_i}\right)tanh\left(\frac{l-l_d}{L_i}\right)+\beta}\right)\right]R_{f,i}$$

Equation 6

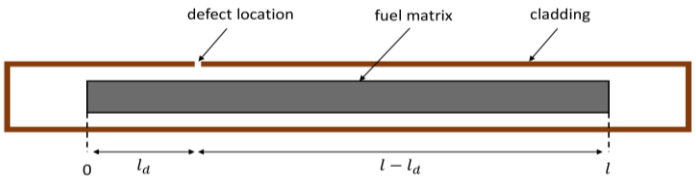

Figure 1. Simple geometric representation of defect location in the cladding.

2.3. Fission Product transport in the Coolant

The FP transport in the coolant can be modelled using the first-order kinetic approach. The source/production term is the release rate from the gap to the coolant, whereas the loss term comprises the decay of radioisotopes and the contribution from different purification systems located in the primary coolant circuit. The mass balance equation for the FP transport in the coolant can be expressed as (Iqbal et al., 2008; Kim & Kim, 2012):

$$\frac{dN_{c,i}}{dt} = R_{g,i} - \left(\lambda_i + \frac{Q}{M}\eta_i + B_{BRS} + \frac{L}{M}\right)N_{c,i}$$

where,
$N_{c,i}$ is the number of atoms of radionuclide i in the coolant region,
$R_{g,i}$ is the release rate of radionuclide i from the gap in s^{-1},
λ_i is the decay constant of radioisotope i in s^{-1},
Q is the letdown flow rate in kgs^{-1},
M is the total coolant mass in kg,
η_i is the resin efficiency for radioisotope i,
B_{BRS} is the removal rate of radionuclide i from boron removal system in s^{-1},
L is the coolant leak rate in kgs^{-1}

The FP activity in the coolant region can also be due to the contribution from tramp uranium contamination resulting from a previous fuel loss from defected fuel elements, or due to defects during the fuel manufacturing process. Such contamination is in the form of fine fuel debris deposited on in-core surfaces. Due to their small particle sizes, the temperature generated by fission heating is generally too low for diffusion to be an important release process and the release by recoil is then the dominant mechanism. The contribution to the release rate into the coolant from the tramp uranium can be determined due to recoil (Lewis, 1987) as presented earlier:

$$\left(\frac{R}{B}\right)^{tramp} = \epsilon_{rec}\left(\frac{S_g}{V}\right)_{tramp}\mu_f$$

where the recoil efficiency is a function of the particle size and the recoil mean free path length. For a particle of size D (m), the efficiency becomes:

$$\epsilon_{rec} = \frac{1}{2}\left(\frac{a}{3\alpha^3} + \frac{1}{2}\left(1 - \frac{1}{\alpha^2}\right)\right)$$

with $a = D/\mu_f$ and $\alpha = max(1, a)$
For a particle of size less than the range of the FP in the fuel ($D << \mu_f$), $\alpha \to 1$ and we get

$$\left(\frac{R}{B}\right)^{tramp} = 1$$

This implies that any FP produced in the tramp uranium will be released to the coolant instantaneously. It is generally assumed that these tramp uranium particles are deposited on the cladding surface and thus only half of the FP with the direction of recoil opposite to the cladding surface will be released, so we have:

$$\left(\frac{R}{B}\right)^{tramp} = \frac{1}{2}$$

So, the release rate from the tramp uranium can be determined as:

$$R_{tramp} = \frac{1}{2} * B$$

Here the birth rate, $B = F_t Y_i$, with F_t being the fission rate of tramp uranium particles and Y_i is the independent fission yield of radioisotope i.

From (Lewis et al., 2017), (R/Y) = 1/2 $F_t \approx$ const ($\approx 1.3 * 10^{12}$ fission/s) was used as a fitted value. However, in the present study, this value will make R_{tramp} of the same order as the $R_{g,i}$. So, in order to have a more significant contribution from $R_{g,i}$ than that from the tramp uranium, we have taken this constant to be of the order of $\sim 10^{10}$ fission/s, considering the tramp uranium contribution to activity as a residual activity present in the coolant. Further investigation would be needed to estimate this value to model the tramp uranium contribution more precisely. Therefore, for the release rate due to tramp uranium, we use the expression:

$$R_{tramp} = 1.3 * 10^{10} * Y_i$$

The R_{tramp} thus evaluated is a source term for the activity of FP in the coolant region and is included in the mass balance equation, which becomes:

$$\frac{dN_{c,i}}{dt} = R_{g,i} + R_{tramp} - \left(\lambda_i + \frac{Q}{M}\eta_i + B_{BRS} + \frac{L}{M}\right) N_{c,i}$$

Equation 7

From the number of atoms of the radioisotopes in the coolant region, we can estimate the activity of those isotopes with the relation:

$$A_{c,i} = \lambda_i * N_{c,i}$$

Equation 8

For the case when there is no defect (intact fuel), or for the duration before occurrence of a defect in the cladding, the source term in the coolant is only due to the tramp uranium contribution. Once the defect occurs, the $R_{g,i}$ term starts contributing to the source term in the coolant and a rise in activity of radioisotopes will be observed.
As seen from the above discussion, the FP transport is governed by different mechanisms in the three regions of Pellet, Gap and Coolant. Several parameters contribute to the release rates from the three regions. These parameters are depicted in their respective regions in Figure 2.

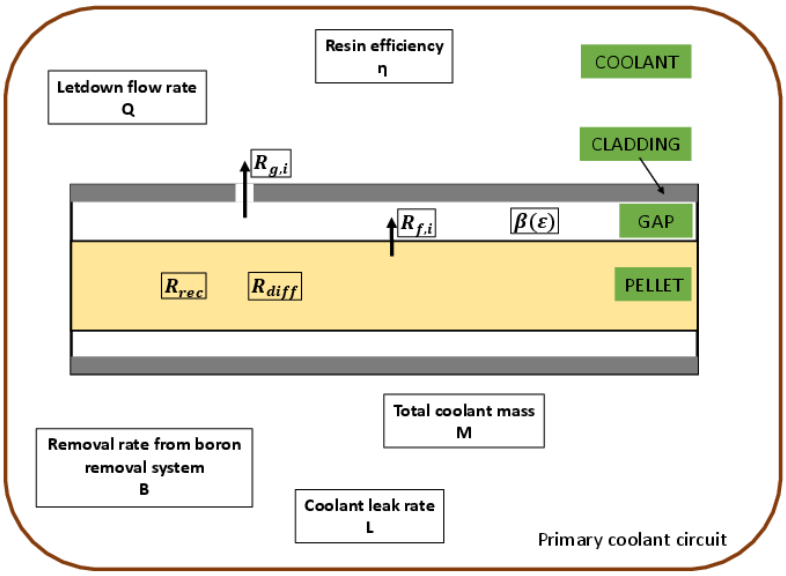

Figure 2. Simple geometric schematic of different parameters contributing to release in the three regions: Pellet, Gap and Coolant.

To summarize, in the present model the FP transport in the pellet region has been considered to be due to the diffusion and recoil mechanisms. The generalized model unifying the diffusion and kinetic modelling approach has been used for the gap region and the first-order kinetic model is used for FP transport in the coolant region.

A schematic diagram representing the production and loss through the three regions and eventual coolant activity estimation is shown in Figure 3.

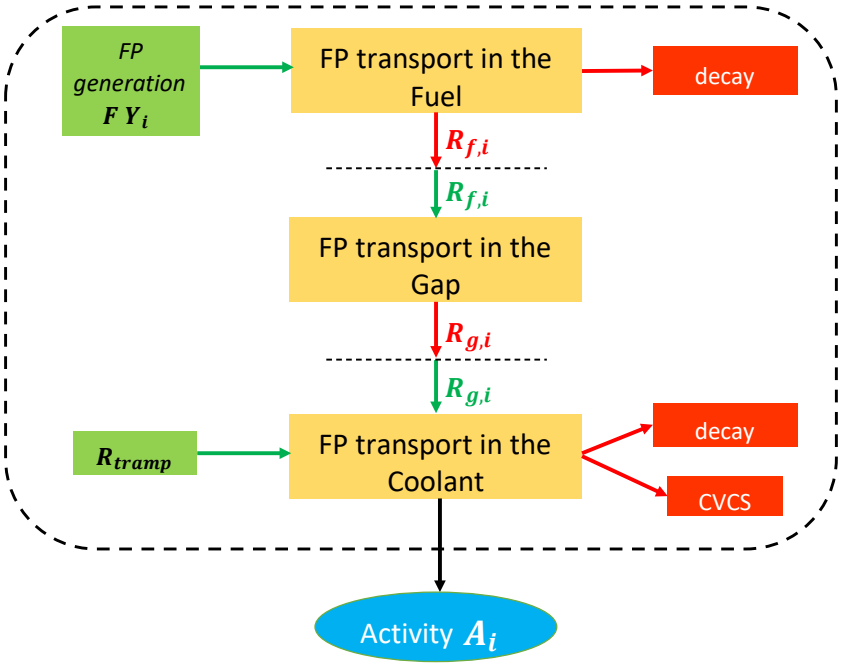

Figure 3. Schematic diagram for production and loss through the Fuel, Gap and Coolant and eventual coolant activity estimation.

2.4. Activity calculation with the Physical Model

The physical model was developed using the mass balance equations in the three regions: Pellet, Gap, and Coolant, to get the estimates of radioisotope activities in the primary coolant. We considered 8 decay chains comprising a total of 30 radioisotopes. These decay chains were considered as they comprised the isotopes of interest such as noble gases (Xe, Kr) and volatile species (I). These isotopes are of interest because of their contribution to the coolant activity and the consequence of radiological exposure if released into the environment. The isotopes of interest include:

- noble gases : Kr-85m, Kr-87, Kr-88, Xe-131m, Xe-133m, Xe-133, Xe-135m, Xe-135
- volatile species : I-131, I-132, I-133, I-134, I-135

The isotopes of the 8 decay chains and their properties are presented in
Table **1**. The (JEFF 3.3, 2017) library is used to get the properties of the various isotopes. These properties include the decay constants of the isotopes, their independent fission yields, location in the decay chain, and the branching fractions. $frac_{12}$ represents the fraction of isotope 1 which disintegrates to isotope 2 in that chain, and so on.

isotope	location in the chain	decay constant (s^{-1})	fission yield	$frac_{12}$	$frac_{13}$	$frac_{23}$	$frac_{24}$	$frac_{34}$	$frac_{35}$	$frac_{45}$
Br-85	1	3.98E-03	0.00249	0.998	0.002	0.0	-	-	-	-
Kr-85m	2	4.30E-05	3.48E-05	0.0	0.0	0.214	-	-	-	-
Kr-85	3	2.04E-09	1.51E-04	0.0	0.0	0.0	-	-	-	-
Br-87	1	1.24E-02	0.01277	0.975	0.0	0.0	-	-	-	-
Kr-87	2	1.51E-04	0.00691	0.0	0.0	1.0	-	-	-	-
Rb-87	3	4.56E-19	8.57E-05	0.0	0.0	0.0	-	-	-	-
Br-88	1	4.20E-02	0.01102	0.933	0.0	0.0	-	-	-	-
Kr-88	2	6.78E-05	0.02064	0.0	0.0	1.0	-	-	-	-
Rb-88	3	6.49E-04	0.00280	0.0	0.0	0.0	-	-	-	-
Te-131m	1	6.42e-06	0.00504	0.21	0.79	0.0	0.0	0.0	-	-
Te-131	2	4.62e-04	0.0252	0.0	0.0	1.0	0.0	0.0	-	-
I-131	3	1.0e-06	0.02921	0.0	0.0	0.0	0.0	0.019	-	-
Xe-131m	4	6.71e-07	0.000317	0.0	0.0	0.0	0.0	0.0	-	-
Sb-132m	1	2.82e-03	0.00869	0.0	1.0	0.0	0.0	0.0	-	-
Sb-132	2	4.15e-03	0.01917	0.0	0.0	1.0	0.0	0.0	-	-
Te-132	3	2.48e-06	0.0429	0.0	0.0	0.0	0.0	1.0	-	-
I-132	4	8.39e-05	0.04317	0.0	0.0	0.0	0.0	0.0	-	-
Te-133m	1	2.08e-04	0.03219	0.175	0.825	0.0	0.0	0.0	0.0	0.0
Te-133	2	9.28e-04	0.03795	0.0	0.0	1.0	0.0	0.0	0.0	0.0
I-133	3	9.22e-06	0.06649	0.0	0.0	0.0	0.0	0.029	0.971	0.0
Xe-133m	4	3.64e-06	0.00192	0.0	0.0	0.0	0.0	0.0	0.0	1.0
Xe-133	5	1.53e-06	0.06653	0.0	0.0	0.0	0.0	0.0	0.0	0.0
Te-134	1	2.76e-04	0.06773	1.0	0.0	0.0	-	-	-	-
I-134	2	2.20e-04	0.07732	0.0	0.0	1.0	-	-	-	-
Xe-134	3	1.99e-24	0.07775	0.0	0.0	0.0	-	-	-	-
Te-135	1	3.65e-02	0.036003	1.0	0.0	0.0	0.0	0.0	0.0	0.0
I-135	2	2.93e-05	0.06064	0.0	0.0	0.1615	0.8349	0.0	0.0	0.0
Xe-135m	3	7.55e-04	0.01178	0.0	0.0	0.0	0.0	0.999	0.0	0.0
Xe-135	4	2.11e-05	0.06206	0.0	0.0	0.0	0.0	0.0	0.0	1.0
Cs-135	5	9.55e-15	0.06314	0.0	0.0	0.0	0.0	0.0	0.0	0.0

Table 1. Properties of the radioisotopes considered in the analysis.

The calculations can be carried out sequentially in the pellet, gap and coolant regions. For the pellet region, the mass balance equations for the different isotopes in a chain form a set of ordinary differential equations corresponding to the usual Bateman equations, with the addition of a sink term. For example, for a 3-isotope chain, the set of equations is:

$$\frac{dN_{f,1}}{dt} = FY_1 P_{lin} l - \lambda_1 N_{f,1} - R_{rec,1} - R_{diff,1}$$

$$\frac{dN_{f,2}}{dt} = FY_2 P_{lin} l + frac_{12}\lambda_1 N_{f,1} - \lambda_2 N_{f,2} - R_{rec,2} - R_{diff,2}$$

$$\frac{dN_{f,3}}{dt} = FY_3 P_{lin} l + \left(frac_{13}\lambda_1 N_{f,1} + frac_{23}\lambda_2 N_{f,2}\right) - \lambda_3 N_{f,3} - R_{rec,3} - R_{diff,3}$$

The set of ordinary differential equations is solved for N_f. The time integration is done using Euler's explicit scheme with forward difference in time. Thus, the time dependent values of N_f for each isotope can be obtained. The release rate from the pellet is obtained for the isotope 'i' using the expression for $R_{f,i}$ in Equation 4.
Next, for the particular case of the gap region, the mass balance equations need not be solved as the release rate from the gap, $R_{g,i}$, can be obtained directly from the expression in Equation 6. So, first the value of β is calculated from the expression in Equation 5 and then β and the $R_{f,i}$ obtained earlier are used in the expression for $R_{g,i}$.
Next, like the pellet region, the set of ordinary differential equations in the coolant region (Bateman equations with additional source and sink terms) are solved for N_c. By carrying out the time integration, as before, the time dependent values of N_c for each isotope in the coolant are obtained. The activity of these isotopes in the coolant can then be calculated by the expression for activity in Equation 8.
The parameters used in the release model for activity calculation and their values are presented in
Table 2. The typical operating values of a PWR are used for the fuel and gap parameters. The remaining parameters (especially concerning the coolant region) were adopted from (Iqbal et al., 2008).

Parameter	symbol	Name used	value	units
fuel stack length	l	-	0.168	m
average linear power	P_{lin}	power	22.77e+03	Wm^{-1}
width of fuel-to-sheath gap	d_{gap}	gap width	24.32e-06	m
radius of pellet	R_{pel}	radius pel	4.15e-03	m
gap internal pressure	P_{int}	Pressure int	15.5e+06	Pa
fission rate	F	-	3.03e+10	fissions $W^{-1}s^{-1}$
location of cladding defect	l_d	defect loc	0.084	m
resin efficiency for Te	η_{Te}	resin eff Te	0.9	-
resin efficiency for I	η_I	resin eff I	0.99	-
resin efficiency for Xe	η_{Xe}	resin eff _Xe	0.9	-
Boltzmann constant	k	-	1.38e-23	JK^{-1}
release rate of H2	q_{H2}	release rate _H2	1e+21	$m^{-3}s^{-1}$
letdown flow rate	Q	letdown flow rate	3.0	kgs^{-1}
total coolant mass	M	tot coolant mass	1.07e+06	kg
BRS removal rate	B	BRS removal rate	1e-05	s^{-1}
coolant leak rate	L	coolant leak rate	2.3e-03	kgs^{-1}
Temperature of ext surface of cladding	T_{clext}	Temp cl ext	597.14	K
Avg. temperature of pellet	T_{pel}	Temp pel	1261.05	K

Table 2. The values of model parameters used in the analysis

The evolutions of the activities of the isotopes of interest in the primary coolant are plotted in Figure 3. The smaller values of activity can be noted up to 10 days, before the occurrence of the defect. These activities in the primary coolant are due to the residual tramp uranium contribution. As soon as the defect occurs, at t = 10 days, the activity values rise for most of the isotopes as in addition to the tramp uranium, the release of those isotopes from the gap to the coolant comes into play. The activity values reach a saturation state for all the isotopes within the duration of the calculation as the source of radioisotopes gets balanced by their decay or by removal through the CVCS purification system in the primary coolant.

The total calculation time was set at 2.5*10^6 s which is approximately 28.9 days. The total time was taken arbitrarily, but large enough to allow the FP activities in the coolant to reach steady-state condition. The time step for the time integration was taken as 40.0 s, which was optimized in order to avoid instability while using the explicit scheme and the defect onset time was set at 8.64*10^5 s, i.e., at 10 days in order to observe distinctively the before and after defect onset regions in the coolant activity curves.

The release to birth ratio, R/B, in the pellet region, as obtained using the physical model, is plotted against the decay constants for the isotopes included in the study in Figure 4(a). The diffusion release and recoil release, along with the total release from the pellet can be noted in the figure. It is observed that R/B exhibits a $\lambda^{-1/2}$ behaviour for the longer-lived isotopes which is indicative of a diffusion-controlled release, whereas R/B is relatively independent of the λ for the shorter-lived isotopes, a behaviour typical of a predominant surface-recoil release.

These results are in accordance with the results observed by sweep gas experiments (Booth, 1957; Lewis, 1987). The R/B vs λ plot for the isotopes of interest, which include the noble gases, like Xe and Kr and the volatile species of I, are shown in Figure 4(b). In accordance with experiments, the R/B is related to the decay constant as $(R/B) \propto \lambda^{-1/2}$ for these range of isotopes.

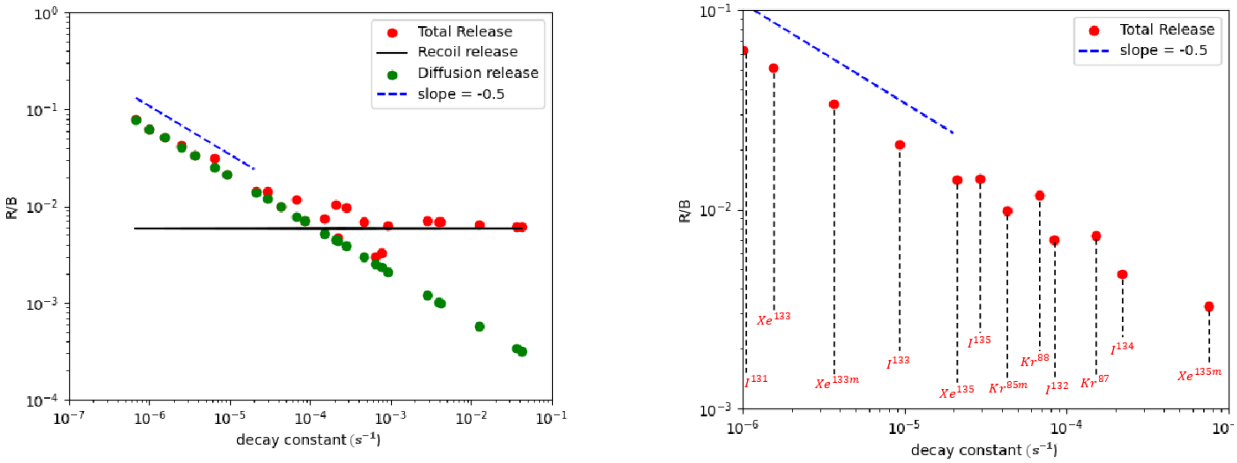

(a) All isotopes (b) Isotopes of interest (Xe, Kr and I).

Figure 4. R/B vs. decay constant for the isotopes in the study in the pellet region.

We note some disturbance for some of the isotopes (in the range $\lambda = 10^{-4} - 10^{-3}$) in the figures which were found to be occurring due to the transmutation of the isotopes and their branching ratios. When the transmutation of isotopes was neglected, by neglecting the branching ratios, the disturbance was gone and a rather smooth curve or transition between long-lived and short-lived isotopes can be observed.

For the gap region, the release to birth ratio, using the physical model, is plotted against the decay constants for the isotopes included in the study in Figure 5. From (Veshchunov, 2019), the different escape regimes were noted for the different isotopes in the gap region: For the long-lived isotopes, $R_{g,i} \propto R_{f,i}$, whereas for the short-lived isotopes, $R_{g,i} \propto R_{f,i}\lambda^{-1}$.

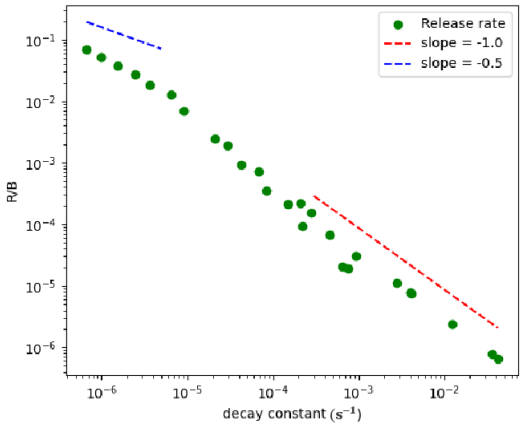

Figure 5. R/B vs. decay constant for the isotopes in the study in the gap region

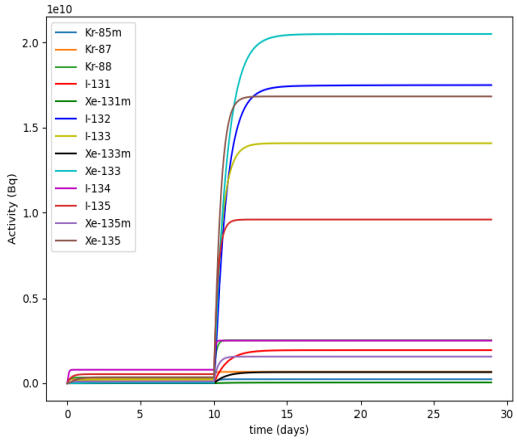

Figure 6. The evolution of the activities of the isotopes of interest in the primary coolant

From the Figure 5 it is evident that for the long-lived isotopes, (R/B) $\propto \lambda^{-1/2}$ which is in accordance with the expression $R_{g,i} \propto R_{f,i}$. Similarly for the short-lived isotopes, (R/B) $\propto \lambda^{-1}$ which is in accordance with the expression $R_{g,i} \propto R_{f,i}\lambda^{-1}$ since $R_{f,i} \propto \lambda^{0}$ for the short-lived isotopes. The different escape regimes observed in the gap region are, thus, in close agreement with the expected observations from literature.

Next, as stated before, we calculate the activity of the various isotopes in the primary coolant. The evolution of the activities of the isotopes of interest in the primary coolant are plotted in Figure 6. The smaller values of activity can be noted up to 10 days, before the occurrence of the defect. These activities in the primary coolant are due to the residual tramp uranium contribution. As soon as the defect occurs, at t = 10 days, the activity values rise for most of the isotopes as the release of those isotopes from the gap to the coolant comes into play, in addition to the tramp uranium. The activity values reach a saturation state for all the isotopes within the duration of the calculation as the source of radioisotopes gets balanced by their decay or by removal through the CVCS purification system in the primary coolant.

From the analysis carried out using the physical model, it is evident that the model operates in the desired or expected manner. Apart from some neglected physical phenomena, the model produces the results which would be deemed necessary for generating the database for the ANN model. Next, we carry out the data sampling and sensitivity analysis of the model parameters.

3. Data Sampling and Parametric Analysis

Now that we have a physical model to calculate the radioisotope activities in the coolant, it is important to have an uncertainty quantification (UQ) and sensitivity analysis (SA) of the model parameters to understand the variability in the output due to uncertainties in the input parameters and the impact of each input parameter on the output variability. This will also allow us to have an estimate of the best predictors (the parameters that influence the output most).

Moreover, the data sampling can be done using the input parameters to get the sample file which will be used with the physical model to arrive at the different output (activity) values.

In our physical model, we identify 16 input parameters (see **Table 3**) which can be varied to carry out the UQ and SA as well as to generate the sample file. We have considered a single decay chain comprising 4 isotopes for this analysis. The concerned decay chain is:

$$^{131m}Te \xrightarrow{yields} {}^{131}Te \xrightarrow{yields} {}^{131}I \xrightarrow{yields} {}^{131m}Xe$$

The primary step for UQ and SA and to create the computational database is to generate a large sample of data. The model calculations are carried out on each data set of the sample to arrive at the output depending on the input data set. We have used an in-house tool, comprising a collection of R (R Core Team, 2022) scripts, to carry out the sampling of the data and for further UQ and SA. The algorithm followed is that first the sampling data is generated using a sample file. Then the physical model described earlier is launched and run 'sample size' number of times, iteratively, with a separate line of the data set of the sample considered in each run. We, thus, obtain the output of the model for each run and they are plotted to see the variability in the output in the different runs. The percentiles are then evaluated to see the range of output variation. Finally, the SA is done using a method depending on the type of sample data.

3. 1. Sample file and dataset generation

The data sampling for the possible input variables are done by using the Transuranus code (Lassmann, 1992) in the statistics mode. By providing the absolute values of parameters, such as the linear power and the outer pin pressure and varying them in a range of 10% in a uniform distribution, we can obtain the equivalent values for parameters such as the pellet centerline temperature, the cladding external temperature, the radius of the pellet and the gap width as outputs. The input parameters obtained by the Transuranus code are the first six parameters in **Table 3**. We generate 2000 samples for these six parameters using the Transuranus code.

Index	Parameter name	Absolute value *(in corresponding SI units)*	Probability law	Range (fraction)	
				Minimum	Maximum
1	power	$22.77*10^{3}$	uniform	0.9	1.1
2	Pressure_int	$15.5*10^{6}$	uniform	0.99	1
3	radius_pel	$4.15*10^{-3}$	-	0.989	1.00
4	Temp_pel	1261.05	-	0.837	1.181
5	Temp_cl_ext	597.14	-	0.973	1.027
6	gap_width	$24.32*10^{-6}$	-	0	2.39
7	defect_loc	0.084	uniform	0	2
8	release_rate_H2	$1.0*10^{21}$	uniform	0.9	1.1
9	letdown_flow_rate	3.0	uniform	0.9	1.1
10	tot_coolant_mass	$1.07*10^{6}$	uniform	0.9	1.1
11	resin_eff_Te	0.9	uniform	0	1.1
12	resin_eff_I	0.99	uniform	0	1
13	resin_eff_Xe	0.008	uniform	0	123.7
14	BRS_removal_rate	$1.0*10^{-5}$	uniform	0.9	1.1
15	coolant_leak_rate	$2.3*10^{-3}$	uniform	0.9	1.1
16	t_defect	$8.64*10^{5}$	uniform	0	2.89

Table 3. The sample file used to generate the sample data.

Next, for the remaining 10 input parameters of the model, the data is randomly sampled using the latin hypercube sampling method. These 10 parameters (indexed 7-16 in **Table 3**) are written into an input (sample) file, along with a probability density function (uniform) and a value for the minimum and maximum for the range of variation in the values of each input. Like before, we vary the absolute values, a priori, in the range of 10%. This file is then fed to

the data sampling tool which generates the 2000 sample data based on the latin hypercube sampling method adopted for sampling.
The generated 2000 samples, comprising different set of values for the 16 input parameters are provided to the physical model as a comma separated value (.csv) file. Each line of the file represents one sample and is used to carry out the calculations of the activity. This is repeated for all the 2000 samples (lines) and we get the output activity values for each such calculation. The computational database for the ANN is thus generated having the 2000 samples with the 16 input parameters as 'features' and the activity of the four isotopes and, separately, the defect status, as 'labels'.

3. 2. Uncertainty Quantification and Sensitivity Analysis

Uncertainty Quantification (UQ) is done to study the variation in the outputs due to the variation (uncertainty) in the input parameters, whereas Sensitivity Analysis (SA) is done to study the importance of each input parameter in terms of its impact on the output. The UQ and SA are generally done in tandem to have a thorough analysis.
For the UQ, we plot the activity values for each of the 2000 calculations. A lot of variation in the activities in the 2000 runs can be observed for the four isotopes of the decay chain. The range of this variation in the outputs can be noted by plotting the different percentiles. The 5^{th} percentile (0.05 curve in the figure) and the 95^{th} percentile (0.95 curve in the figure) allow us to see the range in which 90% of the values lie. The different percentiles are plotted in Figure 7[s] and quiet a wide range of activity values for each isotope could be noted.

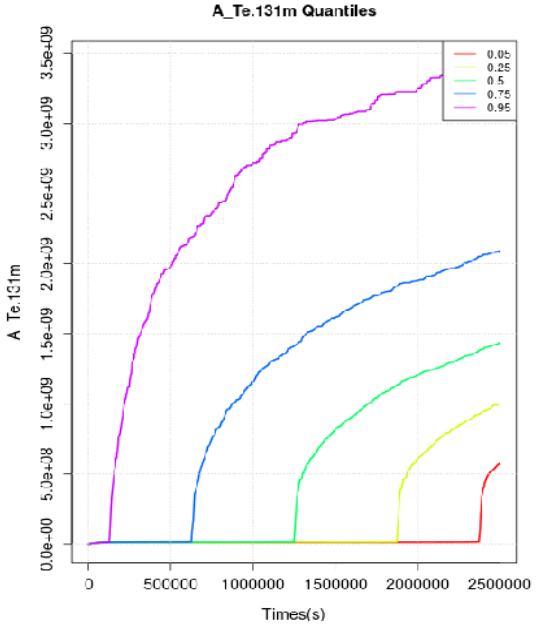

(a) $Te131m$

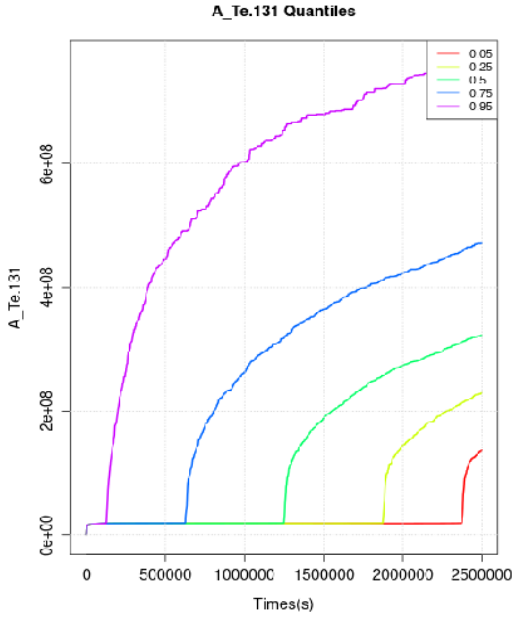

(b) $Te131$

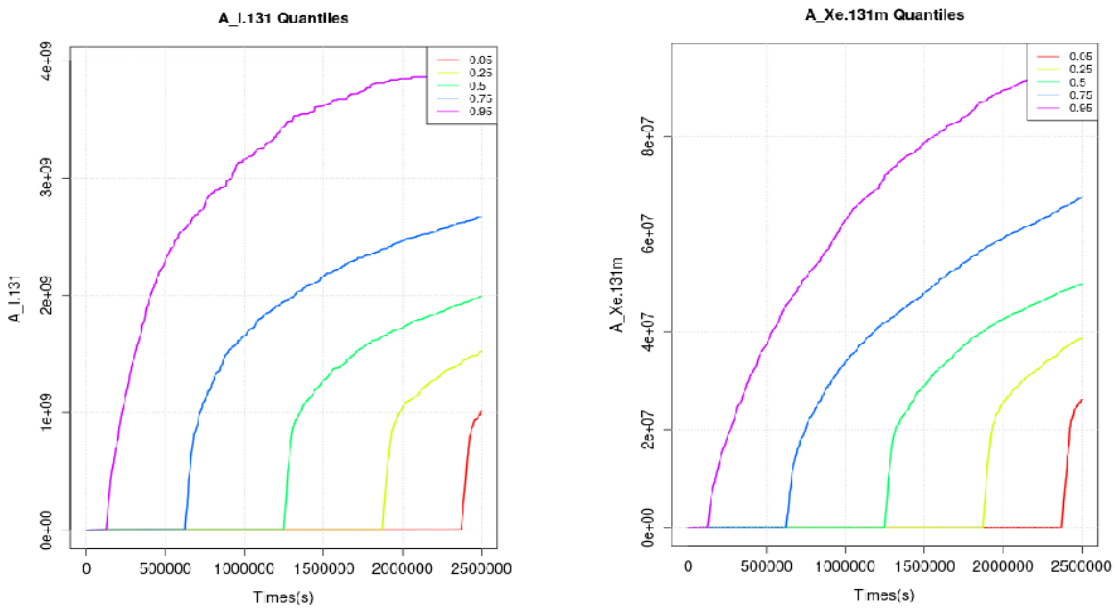

$(c) I131$ $(d) Xe131$

Figure 7. The evolution of the quantiles of activities of the isotopes of interest in the primary coolant.

Now that we have an idea about the variation in the outputs due to uncertainties in the input parameters, it is necessary to carry out a sensitivity analysis to see the effect of each of these input parameters on the outputs. Different methods for the SA can be adopted to get the best estimates of the input parameters that impact the output the most.

First, we check the correlation between the input parameters and the outputs using the partial Pearson correlation coefficient (PCC). PCC is used because simply the Pearson correlation coefficient, which is the ratio of the covariance of two variables and the product of their standard deviations, can be misleading if there is another variable that is numerically related to both the variables of interest. PCC allows us to have a correlation between two variables by ignoring the contributions of the other variables and is thus more precise. Since it is essentially a normalized measurement of the covariance, the result always has a value in the range (-1 ,1). As it only estimates the linear relationship between parameters, it cannot account for the non-linearity or the interaction effects among the input parameters. The PCC estimates can be further corroborated with other SA methods, however, they do provide a broad estimate of the more influential parameters and are used for the analysis in this paper.

The evolution of the correlation coefficients of the 16 input parameters with time using the partial Pearson method for the four isotopes are presented in Figure 8.

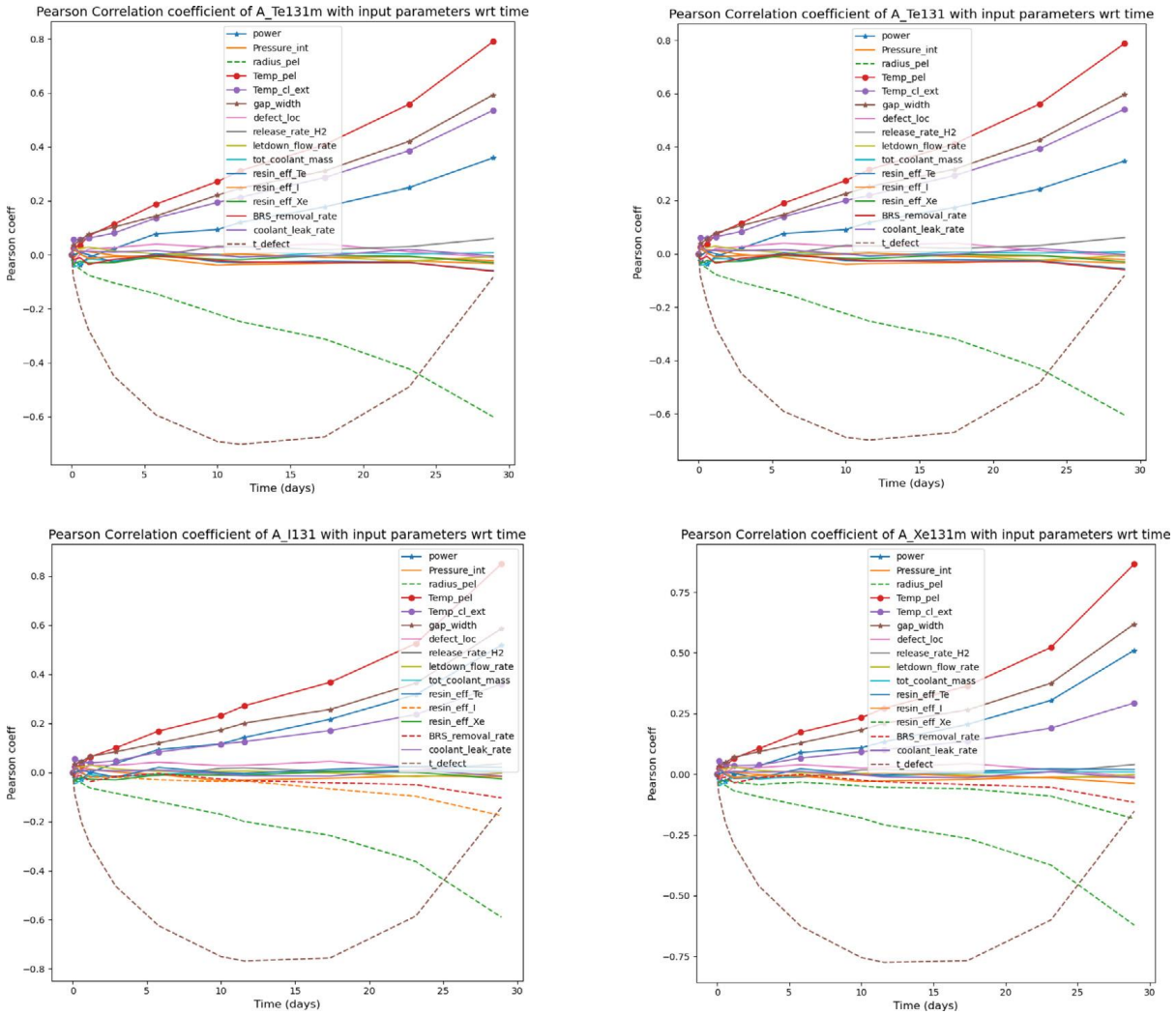

Figure 8. Pearson correlation coefficients for the input parameters with the output for the four isotopes with respect to time.

It can be seen from the figure that some input parameters are correlated more strongly with the output than the others. A PCC of +1 or closer value means a strong positive correlation between the two variables, that is, higher values of one parameter lead to higher values of the other parameter. On the other hand, a PCC of -1 or closer value signifies a strong negative correlation between the two variables, that is, higher values of one parameter lead to lower values of the other. A PCC close to 0 would signify no or a weak correlation between the two parameters.

We identify at least 6 out of the 16 parameters that seem to be more strongly correlated to the activity values for the different isotopes. These parameters are: 'power', 'Temp_pel', 'Temp_cl_ext', 'gap_width', 'radius_pel', and 't_defect'. Out of these, 'power', 'Temp_pel', 'Temp_cl_ext' and 'gap_width' show positive correlation with the activity values and the correlation gets stronger with time. The 'radius_pel' shows a negative correlation with the activity values and gets stronger with time. The 't_defect' parameter also shows a negative correlation with the activity values; however, this correlation varies with time, getting stronger initially and then getting weaker as time progresses. The reason for such striking curve for the 't_defect' can be explained. As the observation for activity values is made at time t = 20 days, if the defect onset happens quickly, i.e., the t_defect is less, the activity will rise and reach a certain high value at t = 20 days. So, a low value of t_defect implies a high value of activity at t = 20 days, and thus a strong negative correlation between the two. As this t_defect increases, the defect onset happens later and thus a rather smaller value of activity is reached at t = 20 days. This explains the strong and progressively stronger negative correlation between the two parameters. After t = 20 days, the t_defect does not have an impact

on the activity value at t = 20 days and thus the correlation between the two variables becomes weaker as is observed in the figures. The other parameters show very less correlation with the output.

These correlations of activities of the isotopes are also justified in terms of the physical model. The activities have a positive correlation with 'power'. The linear power contributes to the birth rate of the radioisotopes in the pellet. From the R/B relations in the pellet, we have R ∝ B, so a higher value of power means a higher value of B which leads to a higher value of the release rate, $R_{f,i}$ from the pellet. A higher $R_{f,i}$ leads to a higher $R_{g,i}$ from the gap to the coolant and eventually to a higher value of the activities in the coolant. Similarly, the activities have a positive correlation with Temp_pel. The parameter Temp_pel occurs in the expression for the diffusion coefficient, D, of the fission products. An increase in Temp_pel exponentially increases the value of D, which in turn is directly proportional to the diffusion release rate, R_{diff}. A higher R_{diff} again implies a higher $R_{f,i}$, which eventually leads to high activity values of the isotopes in the coolant. Next, the activities have a positive correlation with Temp_cl_ext. The cladding external surface temperature is used in the estimation of the surface exchange coefficient, β, in the gap region and a higher value of Temp_cl_ext gives a higher β. Now, β is directly proportional to the release rate from the gap, $R_{g,i}$, so a higher value of Temp_cl_ext leads to a high $R_{g,i}$, which means a higher proportion of radioisotopes in the coolant, contributing to higher activity values. The activities have a positive correlation with gap_width. The width of the radial gap is used to calculate the efficiency of recoil, which is directly proportional to the recoil release rate, R_{rec}. A higher R_{rec} adds to a higher value of $R_{f,i}$ from the pellet, again leading to eventual higher values of the activities in the coolant. Now for the negative correlations of activities, we have the parameters radius_pel and t_defect. The radius of the pellet is used in the expression of the R/B ratio due to recoil and is inversely proportional to R_{rec}. So, a higher value of radius_pel would cause the R_{rec} to decrease causing a decrease in the total release rate from the pellet. So, a lower $R_{f,i}$ will lead to a lower $R_{g,i}$ and eventually to a decreased value of the activities in the coolant. The striking nature of the negative correlation of the activities with t_defect has already been discussed above.

This analysis gives us some idea about the more significant or influential input parameters which affect the output. In other words, it allows us to sort out what is significant and what will be modelled as noise. However, just the correlation of the input parameters with the output may not be sufficient and other SA methods, such as extended Fourier amplitude sensitivity analysis (e-FAST) and Sobol's method, will be adopted in the future to analyse the interactions among the input parameters and their impact on the output.

4. Artificial Neural network

We have generated a computation database comprising the input parameters and the corresponding coolant activities for the four isotopes and also have an initial estimate of the more influential parameters. In this section we will present an Artificial Neural Network (ANN), train it on the computational database and test it against data that is set aside for testing. The development of this ANN is done in Python using the Keras API with TensorFlow backend. We will use what is called the supervised learning for the neural network as it will have both the features and labels in the training set to learn from. First, we use an ANN to train and make predictions about the coolant activity values of the isotopes and later use it to make predictions about the defect status.

4.1 ANN for Activity prediction

Before trying to make a model to estimate the defect characteristics, we develop an ANN to make predictions of the coolant activities by making it learn from the computation database. In order to do so, we consider the 16 input parameters as 'features' and the activity of the 4 isotopes as 'labels' (output). For the moment, the neural network is not time evolving and we take the activity values at a particular instance of time (here at t = 20 days). From the sensitivity analysis performed earlier, we found that 6 input parameters had strong correlation with the activities. In order to carry out the feature selection, i.e., which features would influence the label, we calculate the variance inflation factor (VIF), which is the ratio of the variance of estimating one parameter in a model that includes multiple parameters by the variance of a model constructed using only that one parameter. This gives us an estimate of the measure of co-linearity among the predictor variables. The parameters with a value of VIF more than 5 are expected to be highly co-linear with the other explanatory variables. We used the statsmodels module

(Seabold et al., 2010) in Python for the VIF estimations and found that only 2 other parameters, along with the 6 determined by the sensitivity analysis had VIF > 5. These two parameters were the resin_eff_I and resin_eff_Xe. The feature selection using the VIF estimations and sensitivity analysis of the input parameters, provides us with 8 parameters: 'power', 'Temp_pel', 'Temp_cl_ext', 'gap_width', 'radius_pel', 't_defect', 'resin_eff_I' and 'resin_eff_Xe'. So, we used these 8 input parameters as features and the 4 activity values as labels for the model development. We split the database (2000 samples) into training (80%) set and test (20%) set. So, we have a training set comprising 1600 samples and a test set comprising 400 samples. The test set is kept aside and will serve as never-seen-before data for testing the neural network.

We use a Sequential model, in which the neurons are placed in layers, sequentially. We consider an Input Layer, two Hidden Layers and an Output Layer for the model. The number of neurons in the hidden layers, along with other hyper-parameters of the model, such as batch size, number of epochs, are obtained by tuning these parameters and finding the best parameters. Using a RepeatedKFold cross validation scheme and a Randomized Search on the parameter set, we get the best parameters such that the number of neurons were 36 in each of the two hidden layers, the batch size was 200 and the number of epochs was 10000. A simplified architecture of the ANN for activity predictions is shown in Figure 9.

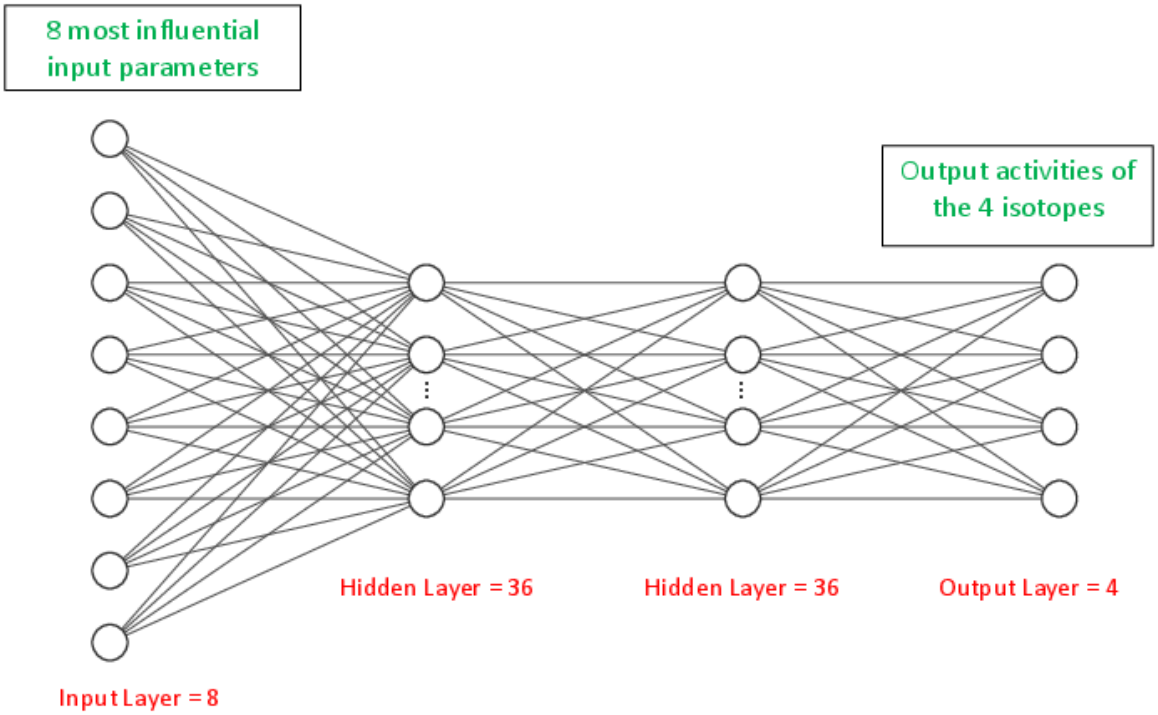

Figure 9. Architecture of ANN for activity prediction.

The other model parameters are also set. We use the 'Adam' optimizer which is a version of the stochastic gradient descent approach. The loss function, that is to be minimized, is taken as the 'mean_squared_error'. The activation function used are 'relu', which gives a positive output (max(0,x)) for a value x. The learning rate is scheduled to evolve using the 'InverseTimeDecay' scheduler. Moreover, 'EarlyStopping' callback is used to avoid unnecessary calculations beyond a certain threshold (monitoring validation loss with patience = 50).
Once the best parameters are known, we create this sequential model and train it on the training set. The model also does a cross-validation along with the training to have a better validation throughout training. The loss curves during the training and validation are plotted in Figure 10.

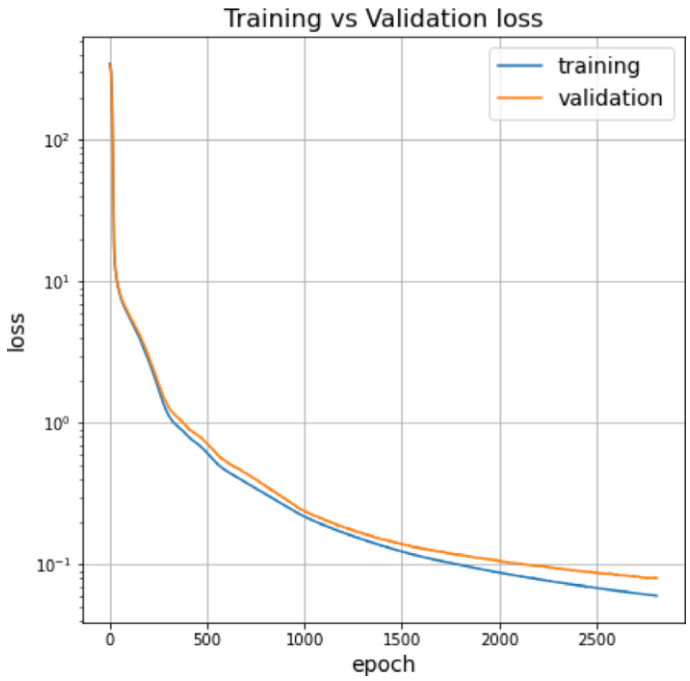

Figure 10. Training vs Validation Loss curve

As expected, we have a decreasing curve for the loss with epochs during both training and validation. This shows that the loss function was minimized until it reached the minimum at which point further training stopped. This was attained in around $\approx$ 2800 epochs (where 1 epoch means one complete pass of the entire training dataset through the algorithm.).

The trained model is then tested on the never-seen-before test data set. Unlike during training, only the features are provided to the neural network, and it makes predictions about the activities of the four isotopes based on its training on the training set. Once we have the predicted values of the activities of the four isotopes, we compare them with the labels of the test set (the real values). We then plot the Prediction vs Reality curves for the normalized values of the activities of the four isotopes. These plots are presented in Figure 11. We find almost linear plots between the activity values predicted by the ANN and the real values of activities from the test data. The R^2 score is quite high (almost close to 1) for all the four isotopes. We observe two distinct sets of data points for the activities. The lower set of activity values represent the observations before the defect onset or onset of defect close to the time of observation (t = 20 days) and the higher set of values represent the observations after the defect onset.

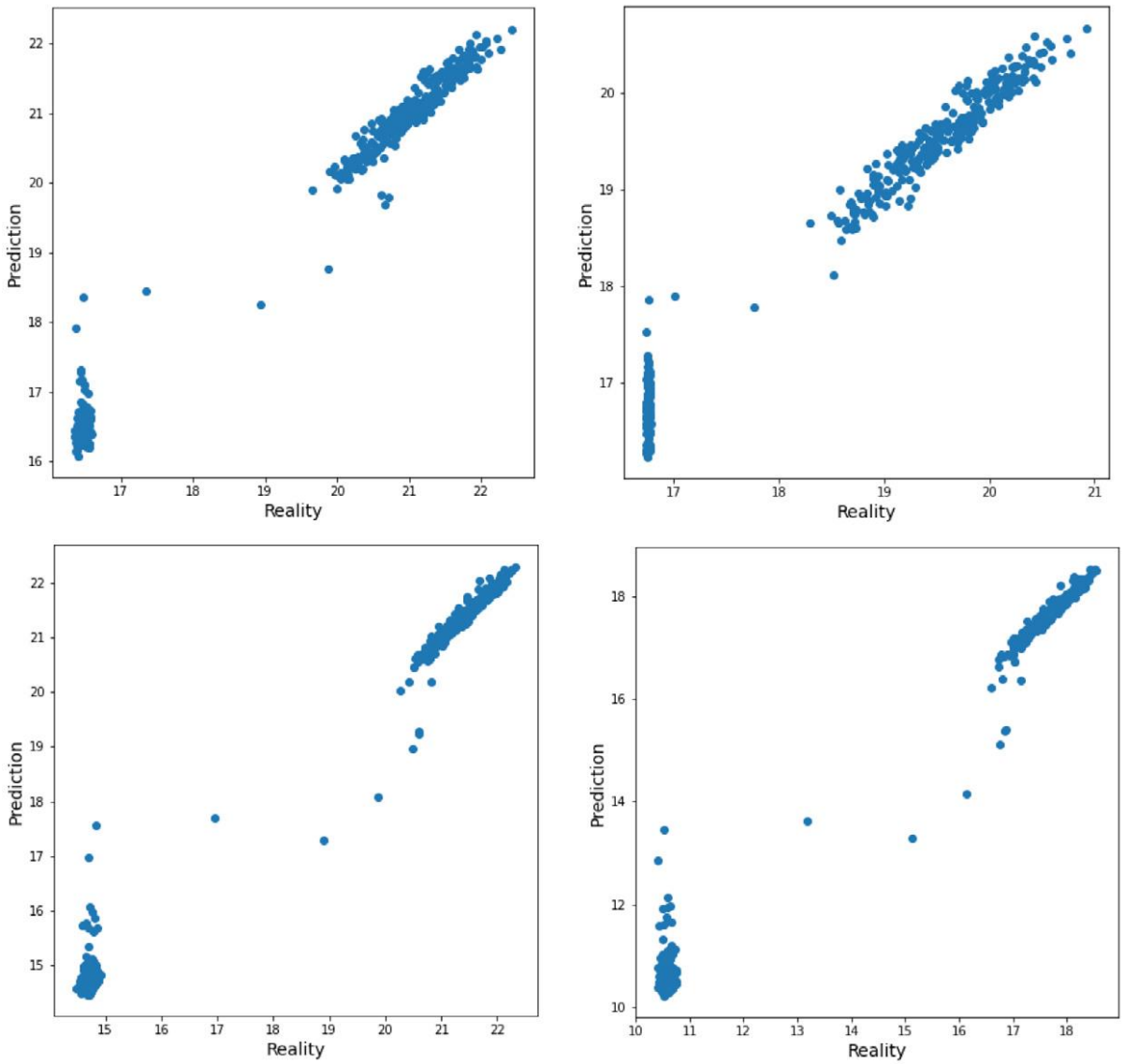

Figure 11. The Prediction vs Reality curves for prediction of activities of the 4 isotopes.

We also note that the higher set of activity values are predicted better than the lower set of values. This difference in prediction accuracy can be noted more precisely from the histogram for prediction and real values of the normalized activities of the four isotopes as presented in Figure 12. There is such a difference because the higher activity values are the ones after defect onset (influence of both $R_{g,i}$ and R_{tramp} as source terms from Equation 7 and are dependent on the significantly correlated input parameters. Such strong correlation between the input parameters and the output activity allows the model to be trained better and make more accurate predictions. On the other hand, the lower set of activities are mostly due to observations before defect onset (only R_{tramp} contribution for the source). Here the problem is ill-poised as the input parameters have rather insignificant effect on the output activity and thus the predictions made by the model are bound to be poor.

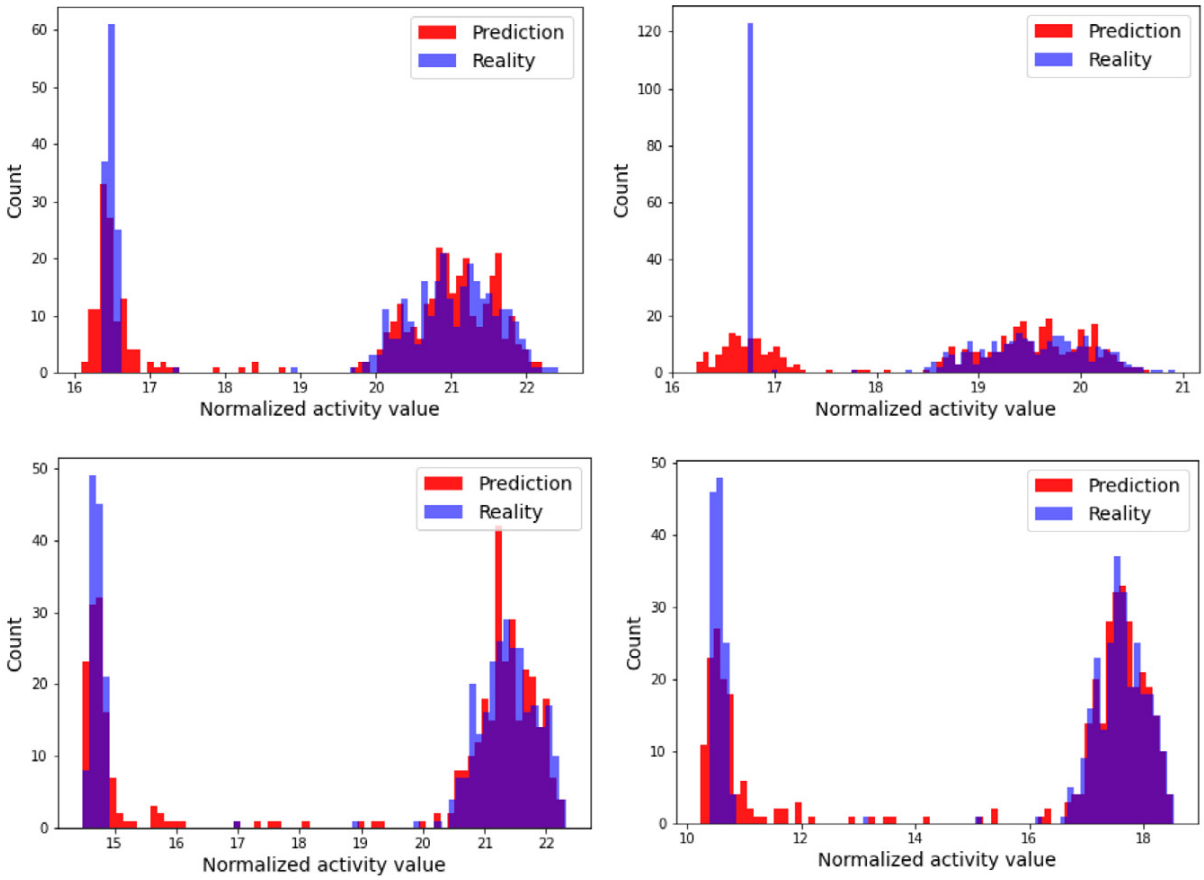

Figure 12. Histograms for Predicted and Real values of normalized activities of the 4 isotopes.

One approach to deal with the poor performance in the lower set of observations would be the segmenting of the training dataset.

The Error Histograms are also plotted for the four isotopes in Figure 13. These represent the error or the difference between the predicted and real values of the activities. It is seen from the figure that the error for majority of the observations lie in the vicinity of 'zero error', proving the good accuracy with which, the predictions have been made by the ANN. Moreover, the correlation between the errors and the input parameters were checked to see if the error was due to any of the input parameters, but no correlation was found, again ascertaining that the model performs well.

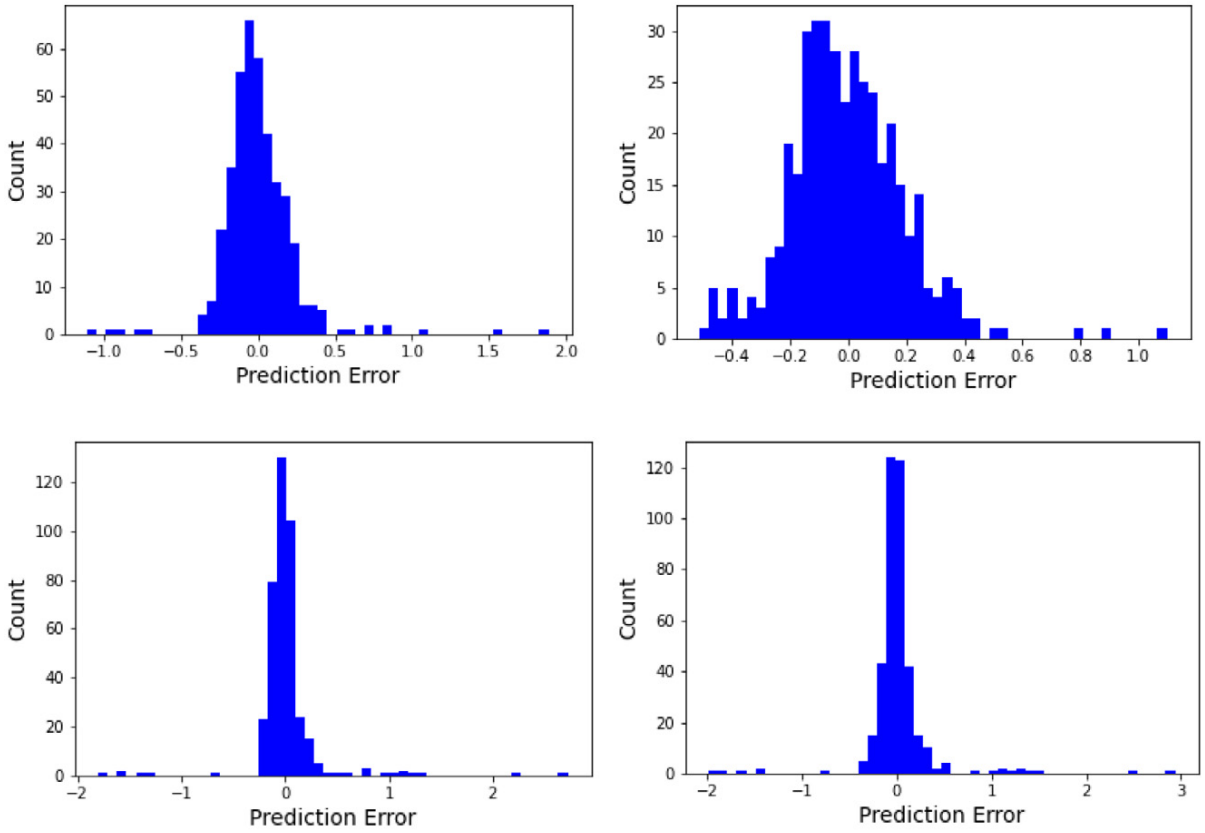

Figure 13. Error Histograms for the 4 isotopes.

So, in this initial analysis, we have developed a neural network that uses supervised learning to make predictions about the coolant activity values. Next, we will use this concept to make predictions about the defect status.

4.2 ANN for defect status prediction

The actual aim of the ANN is to predict the defect status of the fuel rods using the coolant activity values. The defect status prediction can be considered as a classification problem as Defect? Yes(1) or No(0). We will have the coolant activities of the isotopes as inputs and have the output as either 0 or 1. In order to do so, we modify the database to have the defect status as '0' for all the observations before t_defect, time of defect onset, and the defect status as '1' for all the observations after t_defect. Note that we take the activity values at the instance t = 20 days. For the defect status prediction, we have the activities of the four isotopes along with the linear power 'power' (as the linear power would be known from reactor data) as features and the defect status as the label. So, we use 5 features and 1 label for the model development. Same as before, we split the database (2000 samples) into training (80%) set and test (20%) set. The test set is kept aside and will serve as never-seen-before data for testing the neural network.

Again, we adopt a Sequential model considering an Input Layer, two Hidden Layers and an Output Layer for the model. We tune the hyper-parameters using a RepeatedKFold cross validation scheme and a Randomized Search on the parameter set and get the best parameters such that the number of neurons were 5 in the first hidden layer, 10 in the second hidden layer, the batch size was 400 and the number of epochs was 10000. The architecture of the ANN for defect status predictions is shown in Figure 14.

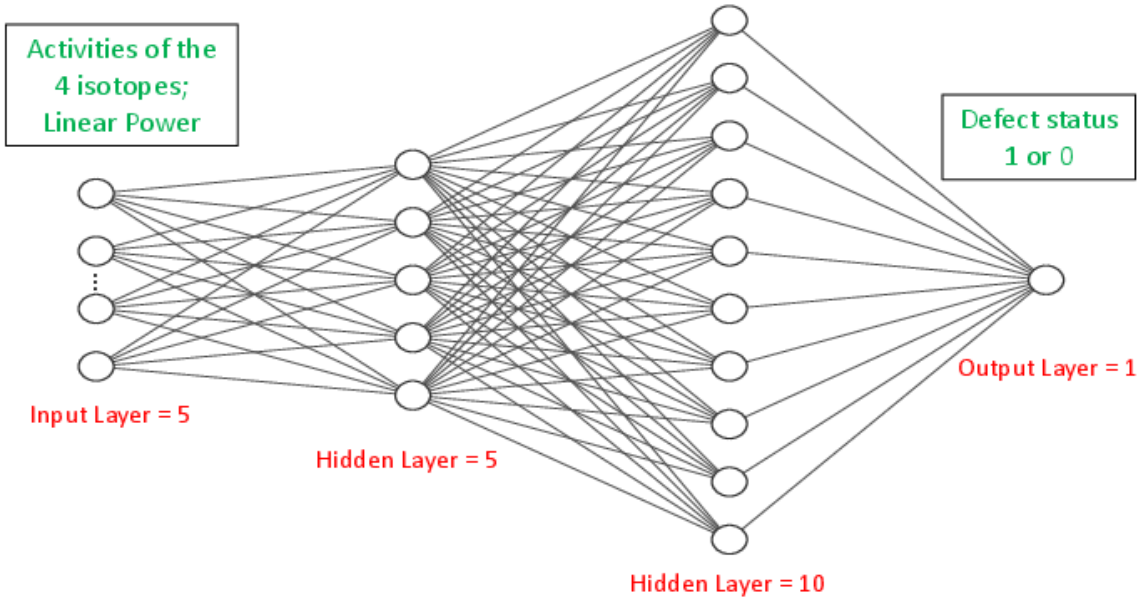

Figure 14. Architecture of ANN for defect status prediction.

The other model parameters are also set. We use the 'Adam' optimizer. For the loss function to be minimized, we take the 'SparseCategoricalCrossentropy'. The activation function used are 'relu', for the two hidden layers and a 'Softmax' function for the output layer. Like the previous case, the learning rate is scheduled to evolve using the 'InverseTimeDecay' scheduler and 'EarlyStopping' callback is used to avoid unnecessary calculations beyond a certain threshold.
Once the best parameters are known, we create this sequential model and train it on the training set. The model also does a cross-validation along with the training to have a better validation throughout training. The loss curve and the accuracy curve during training and validation are presented in Figure 15.

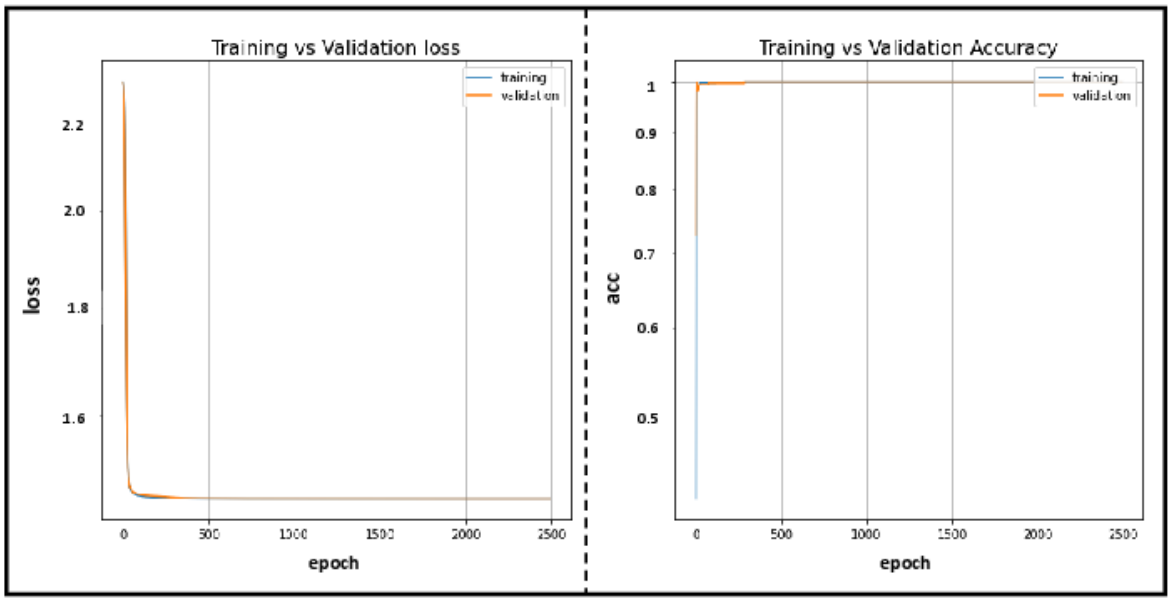

Figure 15. 'Training vs Validation' Loss and Accuracy curves for defect status prediction.

From the Figure 15, we note a decreasing loss curve and an increasing accuracy curve during both training and validation. In fact, the accuracy was found to be 99.5±0.5%. The loss function was minimized until it reached the minimum at which point further training stopped. This was attained in around ≈ 2500 epochs.
The trained model is then tested on the never-seen-before test data set. Only the features are provided to the neural network, and it make predictions about the defect status based on its training on the training set. Once we have the predicted values of the defect status, we compare them with the labels of the test set (the real values). Confusion Matrix is a good visual representation of the performance of classification models like the one used here. It represents the matrix of real and predicted values to present how accurate are the predictions made by the classification model. The confusion matrix is presented in Figure 16.

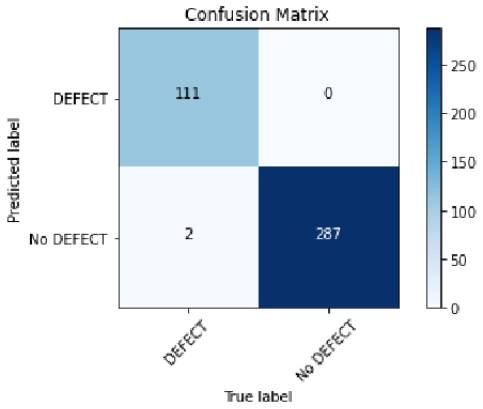

Figure 16. Confusion matrix for the defect status.

The confusion matrix shows that the model very accurately predicted a 'defect' when there actually was a defect and 'no defect' when there actually was no defect. Only for 2 observations out of the 400 samples in the test set, the model predicted a 'no defect' when there actually was a defect. Thus, the defect status can be predicted with the artificial neural network having the coolant activities of the isotopes as input.

4.3 Discussion on ANN

The ANN model developed in this study was used to make predictions about the defect status of a fuel rod during normal operation of a reactor. The inputs to this ANN were the coolant activity values for the different isotopes. In the real-life scenario, the coolant activities are constantly monitored, and a lot of data is obtained. With the limitation to the access to such data, we developed a physical model to generate a computational database of the coolant activities. The good accuracy of defect detection in our model can be attributed to the computation database, which was devoid of any noise or perturbed data. The data from the real reactor may be a lot more discontinuous and with a lot of additional noise. Such database would need to be pre-processed in order to use it with the model. The present model can then be used to make predictions about the defect status based on the data from the real reactors. However, there are several aspects which need to be improved before the ANN can be used with the real data. The defect status prediction was a rather simple classification problem. A more detailed and a regression model would be needed to make predictions about other defect characteristics like the time of defect onset, the defect location, among others. Further analysis to make such predictions using ANN is ongoing.
.

6. Conclusions

During normal reactor operations, it is very important to detect defective fuel since continued operations under defective conditions may lead to operational and economic setbacks for power plants. The activity of isotopes in the primary coolant is a good indicator for defect detection. Among other approaches, Artificial Neural Networks (ANN) have been used to make predictions for the defect detection and characterization of fuel failures. In this paper, a physical model for FP release and activity calculation was developed. This model was intended to be as simplistic yet as accurate as possible. The R/B vs λ curves were plotted for the pellet and gap regions and showed good agreement with experimental results and other models from literature.

The physical model was used to generate a computational database. Sensitivity analysis of the model parameters was carried out to have estimates of the most influential parameters. The most influential parameters were the linear power ('power'), the pellet centerline temperature ('Temp_pel'), cladding external surface temperature ('Temp_cl_ext'), radius of the pellet ('rad_pel'), gap width ('gap_width') and the time of defect onset ('t_defect').

The computational database was used to train and further test the ANN to make predictions, firstly, about the activity of isotopes and then about the defect status. The ANN predicted the activity of the four isotopes with great accuracy (R^2 score > $\approx$ 0.98 for each) and also predicted the defect status with great precision (99.5% accuracy).

The study carried out in this paper is a first step towards the development of an ANN to characterize the defective fuel rods during reactor operation. At present, the ANN deals with a classification problem, whether there is a defect or not. The objective of the ANN would be to make further predictions on the more complex defect characteristics such as the time of defect onset, the location of the defect, among others. The development in this direction is underway. Moreover, the physical model keeps updating to accommodate more physical phenomena and will be improved in the next studies. Finally, the ANN has to be made time evolving as, at the moment, it makes predictions at a particular instance of time. These tasks will be carried out in the future and will be presented in the upcoming publications.

.

References

Abiodun, O. I., Jantan, A., Omolara, A. E., Dada, K. V., Mohamed, N. A., & Arshad, H. (2018). State-of-the-art in artificial neural network applications: {A} survey. *Heliyon*, *4*(11), e00938. https://doi.org/https://doi.org/10.1016/j.heliyon.2018.e00938

Andrews, W. S., Lewis, B. J., & Cox, D. S. (1999). Artificial neural network models for volatile fission product release during severe accident conditions. *J. Nucl. Mater*, *270*(1), 74–86. https://doi.org/https://doi.org/10.1016/S0022-3115(98)00765-X

Awan, S. E., Mirza, S. M., & Mirza, N. M. (2011). Sensitivity analysis of fission product activity in primary coolant of typical {PWR}s. *Prog. Nucl. Energy*, *53*(3), 245–249. https://doi.org/https://doi.org/10.1016/j.pnucene.2010.11.002

Beck, S. D. (1960). *The diffusion of radioactive fission products from porous fuel elements*.

Booth, A. . H. (1957). *A method of calculating fission gas diffusion from UO2 fuel and its application to the x-2-f loop test,AECL-496*. https://www.osti.gov/biblio/4331839-method-calculating-fission-gas-diffusion-from-uo-sub-fuel-its-application-loop-test

Burman, D. L., Correal, O. A., Wilson, H. W., Kunishi, H., & Boman, L. H. (1991). Development of a coolant activity evaluation model and related application experience. *Intern. Topical Meet. Proc. on LWR Fuel Performance*, *1*, 63.

Chun, M. H., Tak, N. Il, & Lee, S. K. (1998). Development of a computer code to estimate the fuel rod failure using primary coolant activities of operating PWRS. *Annals of Nuclear Energy*, *25*(10), 753–763. https://doi.org/10.1016/S0306-4549(97)00126-6

Dong, B., Li, L., Li, C., Zhou, W., Yin, J., & Wang, D. (2019). Review on models to evaluate coolant activity under fuel defect condition in PWR. *Annals of Nuclear Energy*, *124*, 223–233. https://doi.org/10.1016/j.anucene.2018.10.009

Dong, B., Xiao, W., Yin, J., & Wang, D. (2020). Detection of fuel failure in pressurized water reactor with artificial neural network. *Ann. Nucl. Energy*, *140*, 107104.

https://doi.org/https://doi.org/10.1016/j.anucene.2019.107104
Higgs, J. D., Lewis, B. J., Thompson, W. T., & He, Z. (2007). A conceptual model for the fuel oxidation of defective fuel. *Journal of Nuclear Materials*, *366*(1), 99–128. https://doi.org/https://doi.org/10.1016/j.jnucmat.2006.12.050
IAEA. (2019). *Review of Fuel Failures in Water Cooled Reactors (2006–2015)* (Issue NF-T-2.5). IAEA.
Iqbal, M. J., Mirza, N. M., & Mirza, S. M. (2008). Stochastic simulation of fission product activity in primary coolant due to fuel rod failures in typical {PWR}s under power transients. *J. Nucl. Mater*, *372*(1), 132–140.
JEFF 3.3. (2017). *The Joint Evaluated Fission and Fusion File*.
Kim, M.-S., & Kim, K.-T. (2012). Prediction of pellet-to-gap escape and gap-to-coolant release rates of fission products. *Ann. Nucl. Energy*, *49*, 57–69. https://doi.org/https://doi.org/10.1016/j.anucene.2012.06.014
Koo, Y.-H., Sohn, D.-S., & Yoon, Y.-K. (1994). Release of unstable fission products from defective fuel rods to the coolant of a {PWR}. *J. Nucl. Mater*, *209*(3), 248–258.
Lassmann, K. (1992). TRANSURANUS: a fuel rod analysis code ready for use. In H. MATZKE & G. SCHUMACHER (Eds.), *Nuclear Materials for Fission Reactors* (pp. 295–302). Elsevier. https://doi.org/https://doi.org/10.1016/B978-0-444-89571-4.50046-3
Lewis, B. J. (1987). Fission product release from nuclear fuel by recoil and knockout. *Journal of Nuclear Materials*. https://doi.org/10.1016/0022-3115(87)90515-0
Lewis, B. J. (1988). Fundamental aspects of defective nuclear fuel behaviour and fission product release. *Journal of Nuclear Materials*, *160*(2), 201–217. https://doi.org/https://doi.org/10.1016/0022-3115(88)90049-9
Lewis, B. J. (1990). A generalized model for fission-product transport in the fuel-to-sheath gap of defective fuel elements. *J. Nucl. Mater*, *175*(3), 218–226. https://doi.org/https://doi.org/10.1016/0022-3115(90)90210-E
Lewis, B. J., & Bonin, H. W. (1995). Transport of volatile fission products in the fuel-to-sheath gap of defective fuel elements during normal and reactor accident conditions. *J. Nucl. Mater*, *218*(1), 42–56. https://doi.org/https://doi.org/10.1016/0022-3115(94)00372-6
Lewis, B. J., Chan, P. K., El-Jaby, A., Iglesias, F. C., & Fitchett, A. (2017). Fission product release modelling for application of fuel-failure monitoring and detection - An overview. *Journal of Nuclear Materials*, *489*, 64–83. https://doi.org/10.1016/j.jnucmat.2017.03.037
Lewis, B. J., El-Jaby, A., Higgs, J., Thompson, W. T., Iglesias, F. C., Laidler, R., Armstrong, J., Stone, R., & Oduntan, R. (2007). A model for predicting coolant activity behaviour for fuel-failure monitoring analysis. *Journal of Nuclear Materials*, *366*(1), 37–51. https://doi.org/https://doi.org/10.1016/j.jnucmat.2006.11.015
Lewis, B. J., & Husain, A. (2003). Modelling the activity of 129{I} in the primary coolant of a {CANDU} reactor. *J. Nucl. Mater*, *312*(1), 81–96. https://doi.org/https://doi.org/10.1016/S0022-3115(02)01588-X
Lewis, B. J., Iglesias, F. C., Cox, D. S., & Gheorghiu, E. (1990). Model for fission gas release and fuel oxidation behavior for defected ${UO}_2$ fuel elements. *Nucl. Technol.*, *92*(3), 353 – 362. https://doi.org/10.13182/NT90-A16236
Lewis, B. J., MacDonald, R. D., Ivanoff, N. V, & Iglesias, F. C. (1993). Fuel Performance and Fission Product Release Studies for Defected Fuel Elements. *Nucl. Technol.*, *103*(2), 220–245. https://doi.org/10.13182/NT93-A34845
Lewis, B. J., Phillips, C. R., & Notley, M. J. F. (1986). A Model for the Release of Radioactive Krypton, Xenon, and Iodine from Defective UO2 Fuel Elements. *Nucl. Technol.*, *73*(1), 72–83. https://doi.org/10.13182/NT86-A16203
Lewis, B. J., Szpunar, B., & Iglesias, F. C. (2002). Fuel oxidation and thermal conductivity model for operating defective fuel rods. *J. Nucl. Mater*, *306*(1), 30–43. https://doi.org/https://doi.org/10.1016/S0022-3115(02)01231-X
Li, H., Fu, Y., Mao, L., & Mei, Q. (2017). Research on Estimating Methods and Application of Fuel Rods Defect. *International Conference on Nuclear Engineering*, *57816*, V003T02A021.
Likhanskii, V., Afanasieva, E., Sorokin, A., Evdokimov, I., Kanukova, V., & Khromov, A. (2006). *Failed fuel diagnosis during {WWER} reactor operation using the {RTOP-CA} code*.
Lusanova, L., Miglo, V., & Slavyagin, P. (2001). Fundamental principles of failed fuel detection concepts on nuclear power units of {WWER} type. *International Conference on WWER Fuel Performance, Modelling and Experimental Support*.
Manzel, R., & Walker, C. T. (2002). EPMA and SEM of fuel samples from PWR rods with an average burn-up of around 100 MWd/kgHM. *J. Nucl. Mater*, *301*(2), 170–182. https://doi.org/https://doi.org/10.1016/S0022-3115(01)00753-X
Olander, D. R. (1976). *Fundamental Aspects of Nuclear Reactor Fuel Elements*. U.S. Department of Energy Office of Scientific and Technical Information. https://www.osti.gov/servlets/purl/7343826
R Core Team. (2022). *R: A Language and Environment for Statistical Computing*. https://www.r-project.org/
Seabold, Skipper, & Perktold, J. (2010). statsmodels: Econometric and statistical modeling with python. *9th Python*

in Science Conference.

Tayefi, S., & Pazirandeh, A. (2014). Using {H}opfield neural network to optimize fuel rod loading patterns in VVER/1000 reactor by applying axial variation of enrichment distribution. *Applied Soft Computing*, *21*, 501–508. https://doi.org/https://doi.org/10.1016/j.asoc.2014.03.018

Tigeras Menéndez, M. A. (2009). *Fuel Failure Detection, Characterization and Modelling: Effect on Radionuclide Behaviour in PWR Primary Coolant*. 780.

Tigeras Menéndez, M. A., Ambard, A., Laugier, F., Delcoigne, F., Muller, A., & Fizammes, N. (n.d.). Merlin : modeling fuel defects at EDF power plants.pdf. *International Conference on Water Chemistry of Nuclear Reactor Systems, 2004. San Francisco.*

Turnbull, J. A., Friskney, C. A., Findlay, J. R., Johnson, F. A., & Walter, A. J. (1982). The diffusion coefficients of gaseous and volatile species during the irradiation of uranium dioxide. *J. Nucl. Mater.*, *107*(2), 168–184. https://doi.org/https://doi.org/10.1016/0022-3115(82)90419-6

Verma, L., Noirot, L., & Maugis, P. (2020). Modelling intra-granular bubble movement and fission gas release during post-irradiation annealing of {UO2} using a meso-scale and spatialized approach. *J. Nucl. Mater.*, *528*, 151874. https://doi.org/https://doi.org/10.1016/j.jnucmat.2019.151874

Veshchunov, M. S. (2019). Mechanisms of fission gas release from defective fuel rods to water coolant during steady-state operation of nuclear power reactors. *Nuclear Engineering and Design*, *343*(November 2018), 57–62. https://doi.org/10.1016/j.nucengdes.2018.12.021

Wallace, C., McEwan, C., West, G., Aylward, W., & McArthur, S. (2020). Improved Online Localization of {CANDU} Fuel Defects Using Ancillary Data Sources and Neural Networks. *Nucl. Technol.*, *206*(5), 697–705. https://doi.org/10.1080/00295450.2019.1697174

Wei, X., Wan, J., & Zhao, F. (2016). Prediction study on {PCI} failure of reactor fuel based on a radial basis function neural network. *Science and Technology of Nuclear Installations*, *2016*. https://doi.org/https://doi.org/10.1155/2016/4720685

Zanker, H. (1989). Defective fuel rod detection in operating pressurized water reactors during periods of continuously decreasing fuel rod integrity levels. *Nucl. Technol.*, *86*(3), 239 – 247. https://doi.org/10.13182/NT89-A34292